High-Lignin-Containing Cellulose Nanofibrils from Date Palm Waste Produced by Hydrothermal Treatment in the Presence of Maleic Acid

Amira Najahi, Quim Tarrés, Marc Delgado-Aguilar, Jean-Luc Putaux, Sami Boufi

pubs.acs.org/Biomac

Article

High-Lignin-Containing Cellulose Nanofibrils from Date Palm Waste Produced by Hydrothermal Treatment in the Presence of Maleic Acid

Amira Najahi, Quim Tarrés, Marc Delgado-Aguilar,* Jean-Luc Putaux, and Sami Boufi*

Cite This: *Biomacromolecules* 2023, 24, 3872−3886

Read Online

ACCESS | Metrics & More | Article Recommendations | Supporting Information

ABSTRACT: Lignin-containing cellulose nanofibrils (LCNFs) have attracted great attention because the presence of lignin brought additional merits to cellulose nanofibrils including hydrophobicity, ultraviolet (UV)-shielding capacity, and reduced water sensitivity. In the present work, LCNFs with lignin content up to 21 wt % were prepared with a high yield exceeding 70 wt %, from neat date palm waste, by a hydrothermal treatment (HTT) at 120−150 °C in the presence of 20−30 wt % maleic acid, followed by high-pressure homogenization. The chemical composition, degree of polymerization, morphology, and colloidal and rheological properties of the LCNFs were investigated to understand how the HTT in the presence of MA affected the properties of the resulting LCNFs. Nanopapers prepared from the LCNF suspensions exhibited mechanical properties lower than those from lignin-free CNF-based nanopapers, yet with decreased hydrophilicity. A mechanism explaining how the HTT in the presence of MA facilitated the disintegration of the biomass into nanoscale material was proposed. Overall, the present work demonstrated a feasible and scalable approach for the sustainable production of LCNF suspensions from neat agricultural residues, with a high yield and a high lignin content, without any need to perform a preliminary partial delignification.

1. INTRODUCTION

Over the past decade, lignin-containing cellulose nanofibrils (LCNFs) have garnered significant interest as a new class of nanosized lignocellulosic material that could expand the domains of application of nanocelluloses. The presence of lignin in LCNFs likely imparts specific properties, including ultraviolet (UV)-absorption, antioxidant activity, hydrophobicity, barrier properties, and emulsification improvement in Pickering emulsions, among others.[1,2] Numerous studies have demonstrated the beneficial effects of the presence of residual lignin on the reduction of hydrophilicity, water uptake, and water permeability of nanopapers, particularly when the lignin content exceeded 15 wt %.[3,4] For example, thin films of high-lignin content CNFs (23 wt %) were reported to be suitable for producing low oxygen permeability films with an oxygen transmission rate (OTR) comparable to commercially available polymers like poly(ethylene terephthalate) (PET).[5] Other applications encompass the use of LCNFs as an emulsifying agent for oil-in-water (O/W) Pickering emulsions, being an attractive alternative to synthetic surfactants.[6] Furthermore, the presence of lignin has also been reported to be beneficial as a compatibilizer for hydrophobic polymers, and potentially improve their dispersion in composite materials, avoiding the need of using compatibilizers or chemical modification of the reinforcing agent, particularly for nanosized fillers.[7] Remarkably, the incorporation of LCNFs into pulp slurries for the production of brown-line paper has been reported to be more beneficial than lignin-free CNFs, as the enhancement of the mechanical properties is of the same magnitude, but the presence of hydrophobic constituents (i.e., lignin) palliates the negative effect that such high surface area and nanosized material imparts over the drainability of pulp during paper production.[4]

The preservation of lignin is highly recommended in terms of resource utilization. This concept is similar to high-yield pulping in papermaking, where most of the lignocellulosic constituents are preserved, limiting the use of chemical reagents and, thus, minimizing the generation of residual effluents. Interestingly, the preservation of lignin takes advantage of the knowledge on high-yield pulping by breaking down the lignocellulose structure into lignin-rich nanofibrils.[8,9] This approach is particularly valuable for residual biomass feedstocks, such as agricultural residues, which are typically

Received: May 23, 2023
Revised: July 16, 2023
Published: July 31, 2023

discarded but can be valorized in the form of high-performance materials.[10−12]

In lignocellulosic fibers, lignin forms a rigid amorphous matrix embedding hemicelluloses and cellulose fibrils, conferring structural rigidity to fibers and resistance to chemical, microbial, or enzymatic attack, while acting as a natural binder between the rest of the constituents.[13] Lignin is tightly bound to hemicellulose and cellulose through non-covalent and covalent linkage including benzyl ester, benzyl ether, and glycosidic and acetal bonds.[14,15] Owing to the complex three-dimensional network architecture of lignin and structural organization within the lignocellulosic fibers, the traditional methods for CNF production involving chemical and/or enzymatic pretreatments are highly recommended. The suppression of this stage could be detrimental for fibrillation equipment, such as high-pressure homogenizers or microfluidizers, as pressure chambers could become clogged and/or energy consumption would be excessive.[16] Therefore, a chemical pretreatment combined with a mechanical disintegration is a prerequisite for preparing CNFs. Owing to the hierarchical structure of lignocellulosic fibers, the resulting quality of LCNFs, in terms of morphology, rheology, colloidal stability, and usefulness, can be easily tailored by adjusting the intensity of both pretreatments and fibrillation.[17] However, chemistry-based pretreatments usually encompass the oxidation and/or partial dissolution of lignin, thus decreasing its content and limiting the abovementioned advantages of lignin, on the one hand, and decreasing the yield of the whole operation, on the other.[3,18]

The most widely studied chemical pretreatment to facilitate the disintegration of lignocellulosic fibers into LCNFs is TEMPO-mediated oxidation, which was initially used on bleached delignified cellulose pulps to reduce the energy consumption during high-pressure homogenization (HPH).[19] For instance, Herrera et al. used a semichemical pulp containing 26 wt % lignin as feedstock for TEMPO-oxidized LCNFs. At the end of the process, the lignin content accounted for 23 wt %.[5] Their method involved a refining treatment to enhance pulp defibrillation before TEMPO-mediated oxidation to achieve a carboxyl content of around 900 μeq g^{-1}, followed by high-pressure microfluidization. A similar approach was adopted by Wen et al. to produce LCNFs from a high-yield pulp, where the lignin content decreased at increasing extent of oxidation.[20] In our previous work, LCNFs were prepared from date palm waste (DPW) using TEMPO-mediated oxidation of neat DPW as a pretreatment followed by HPH. These LCNFs exhibited a higher thermal stability and a lower hydrophilicity than bleached CNFs, and demonstrated a high reinforcing potential when incorporated into an acrylic polymer matrix via casting.[21]

The combination of a sodium hydroxide or sulfuric acid treatment at low concentration (from 3 to 5 wt %) followed by ball milling and ultrasonication was successfully used to prepare LCNFs from agricultural residues, namely sunflower stalks and reed straw.[22,23] Other approaches, including partial bleaching of a commercially available mechanical pulp from pine, have been also reported to effectively produce LCNFs as a reinforcing agent in papermaking.[18]

Other methods involving chemical, physical, or enzymatic pretreatments have been also reported for LCNF production. A combination of mild sulfonation pretreatment and ultrafine wet grinding at moderate temperature (around 85 °C) was successfully used to produce LCNFs with a high lignin content (around 25 wt %) and a significant reinforcement of paper.[24] Laccase enzymes, which are multi-copper enzymes capable of catalyzing the direct oxidation of a wide range of aromatic compounds such as lignin monomers, were recently used in combination with endoglucanases as a pretreatment of unbleached eucalyptus kraft pulp to produce LCNFs through grinding. This resulted in LCNFs with a broad width distribution (30−100 nm) as well as microscale fibrils.[25]

Deep-eutectic solvents (DESs) have also been explored for the preparation of LCNFs. For example, LCNFs derived from corncob were produced by combining DESs and enzymatic hydrolysis, followed by HPH. The DES treatment selectively removed a fraction of lignin and hemicelluloses, while the enzymatic hydrolysis promoted the disintegration of the cell wall by partial breakdown of the disorganized regions of cellulose.[12] Other approaches involving the use of DESs usually result in low-lignin content CNFs, as these solvents are commonly used to extract and separate hemicelluloses and lignin or promote enzymatic saccharification.[26,27]

Recently, LCNFs with various lignin contents were successfully produced using an innovative approach based on the treatment of lignocellulosic plant biomass with *p*-toluenesulfonic acid (*p*-TsOH), and a dicarboxylic acid, as acid hydrotropes followed by HPH or microfluidization.[28] Since they combine the properties of acids and hydrotropes, acid hydrotrope molecules are capable of cleaving ether and ester bonds from lignin to carbohydrates, thus solubilizing it.[29] By properly adjusting the concentration of the hydrotrope, contact time, and temperature, the lignin content can easily be controlled. Using this approach, *p*-TsOH LCNFs from birch wood were produced by microfluidization at a concentration of 20 wt % *p*-TsOH at 80 °C for 20 h.[30] The same approach was applied to sugarcane bagasse powder (SBP), where LCNFs with a lignin content ranging from 4.69 to 17.53 wt % were obtained by *p*-TsOH and hydrolysis, followed by HPH. Although high lignin contents were found to prevent fibrillation, as the fiber width was markedly higher, the water contact angle of the resulting films significantly increased with increasing lignin content.[31]

Maleic acid has previously been successfully used for the production of lignin-containing cellulose nanocrystals (LCNCs) and LCNFs using unbleached mixed hardwood chemical pulps of lignin contents of 3.9 and 17.2 wt %. A minimum maleic acid (MA) concentration of 50 wt % and a temperature of 100−120 °C were required to produce LCNFs with a high yield and at the nanoscale.[32] The same approach has been applied to bleached eucalyptus pulp (BEP), where carboxylated CNCs and CNFs were produced by MA hydrolysis.[33]

The present work aims at assessing the suitability of using a two-stage hydrothermal treatment (the first one in water, and the second one in the presence of MA), followed by a moderate HPH sequence, to successfully produce chemically derived LCNFs while preserving a high lignin content and assess their characteristics and the performance of LCNF films.

2. EXPERIMENTAL SECTION

2.1. Materials. Date palm waste (DPW) encompassing a mixture of leaflets, leaves, and rachis was used as biomass feedstock to produce LCNFs. It was obtained from the annual pruning of the plant in the oasis region of Gabes, in south Tunisia. Maleic acid (MA) and other chemicals were purchased from Sigma-Aldrich (Spain), and were used

https://doi.org/10.1021/acs.biomac.3c00515
Biomacromolecules 2023, 24, 3872−3886

Scheme 1. Preparation Strategy of LCNFs from DPW by MA Treatment and High-Pressure Homogenization

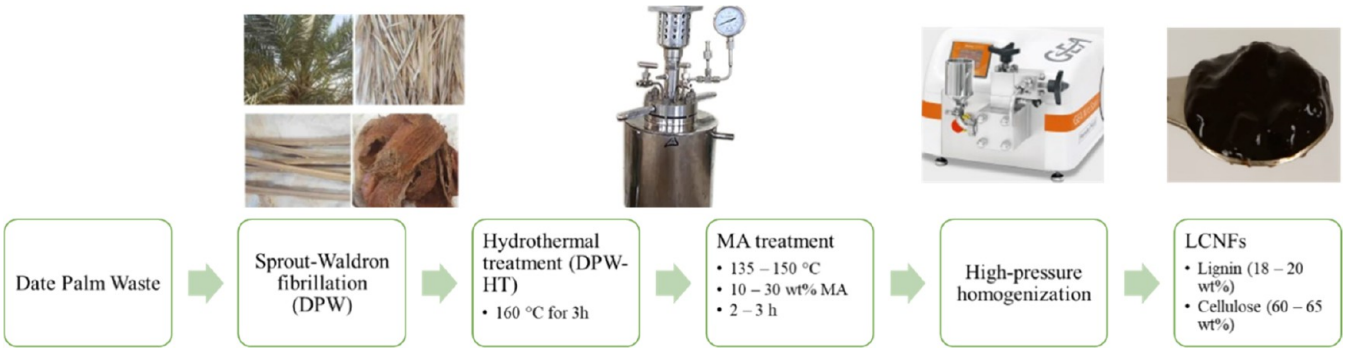

without further purification. Deionized water (DI) was used for all treatments.

2.2. General Procedure. Scheme 1 provides a general overview of the selected strategy for LCNF preparation from DPW, encompassing pretreatment and HPH fibrillation.

2.3. Biomass Pretreatment and LCNF Preparation. DPW was milled and sieved using a knife mill from Agrimsa (Spain) equipped with a sieve of 5 mm at the bottom. The biomass was then fibrillated using a Sprout-Waldron refiner, increasing the surface area and promoting the efficiency of the subsequent chemical treatments. This process was repeated 3 times in order to obtain a constant measure of the fiber diameter in the MorFi equipment. The resulting DPW fibers were subjected to a hydrothermal treatment (HTT) in a stainless-steel jacketed rotary reactor equipped with temperature control. The HTT was carried out by soaking 500 g of fibrillated DPW in 5 L of DI at a solid to liquid ratio of 1:10 and introducing the suspension into the reactor, preheated at 80 °C. The reactor was then sealed, and the temperature was increased to 160 °C. These conditions were maintained for 3 h. The reactor was then cooled down and discharged once the atmospheric pressure inside the reactor was achieved. The suspension was then filtered to obtain a pulp at 50 wt % consistency.

The MA treatment was run as follows in a 3 L jacketed pressurized reactor. In a typical experiment, 300 g of the HTT-treated DPW was introduced and an appropriate volume of MA solution was added so that the solid to liquid ratio was kept at 1:10. Then, the temperature was increased (135 or 150 °C) and the mixture was kept under mechanical stirring for a given time between 2 and 3 h, depending on the selected conditions. After this treatment, the suspension was recovered by filtration through a 10 μm polyamide screen fabric and thoroughly washed with water until achieving neutral pH at the filtrate. In order to identify different samples, the nomenclature MxTytz was adopted, where x, y, and z represent the MA concentration (in wt %), treatment temperature (in °C), and time (in h), respectively.

The fibrillation of the MA-treated pulp was conducted in a PANDA Plus 2000 high-pressure homogenizer (GEA Niro Soavi, Italy) at 1.5 wt % consistency and subjecting the pulp to 3 passes at 300 bar and 3 passes at 600 bar. The resulting LCNFs were stored in hermetic plastic bags at 4 °C for further characterization and use.

2.4. Chemical Composition. The chemical composition of the mechanically treated DPW and all produced samples was determined. First, samples were prepared for chemical characterization according to TAPPI standard T257. Once conditioned, one portion (2 dry g) was used for determining the ash content in an electric muffle furnace, placing the samples in porcelain crucibles and slowly increasing the temperature (2 °C min^{-1}) from 100 to 525 °C. This assured the complete carbonization of the samples without flaming. The crucibles were removed from the furnace when no black particles were observed, and ash was calculated according to eq 1

$$\text{ash} = \frac{w_f}{w_i} \times 100 \tag{1}$$

where w_f is the final weight after combustion and w_i is the initial dry weight of the sample.

In parallel, the samples were subjected to solvent extractive determination, on the one hand, and to $NaClO_2$ bleaching, on the other. In the case of the former, samples (5 dry g) were placed in extraction thimbles for Soxhlet extraction using an ethanol−toluene mixture as a solvent, as detailed in TAPPI standard T204. Samples were submitted to extraction for 5 h in the presence of 150 mL of the ethanol−toluene mixture. Then, the extract was dried at 105 °C in an oven until constant weight. A blank test was also carried out, using the solvent without the sample inside the thimbles. The extractive content was then determined according to eq 2.

$$\text{extractives} = \frac{w_e - w_b}{w_i} \times 100 \tag{2}$$

where w_e and w_b are the final weights of the oven-dry extract and the blank residue, respectively.

The solvent-free samples were then subjected to acid-insoluble lignin determination, according to TAPPI standard T222. Two samples (2 dry g) were placed in 100 mL beakers, where 40 mL of cold (10 °C) 72% sulfuric acid was added, keeping the beakers in an ice bath to prevent sample heating. After the H_2SO_4 addition, the beakers were covered with a watch glass and kept at 20 °C for 2 h. The beakers were manually agitated frequently to ensure complete dissolution. The content of the 100 mL beakers was then transferred into Erlenmeyer flasks containing 400 mL of deionized water, adding extra water until achieving a concentration of sulfuric acid of 3%, and boiled for 4 h. Water was added frequently to maintain the initial volume. The flasks were left inclined overnight to promote lignin precipitation and filtered in a 0.22 μm PVDC membrane, using hot water to wash the cake and remove free acid. Acid-insoluble lignin, present at the top of the membrane, was then dried at 105 °C until constant weight. The acid-insoluble lignin content was then calculated according to eq 3.

$$\text{lignin} = \frac{w_l}{w_i} \times 100 \tag{3}$$

where w_l is the oven-dry weight of lignin.

On the other hand, the original samples were prepared according to the methodology reported by Wise.[34] Briefly, 4 g of the sample was immersed in 160 mL of deionized water, together with 1.5 g of $NaClO_2$ and 0.5 mL of glacial CH_3COOH. The mixture was boiled for 1 h and repeated several times, in terms of adding both $NaClO_2$ and CH_3COOH and keeping the sample for reflux during 1 h, until the residue was perfectly white. This residue, corresponding to holocellulose, was then dried and referred to the initial dry weight of the sample. This lignin-free sample, i.e., holocellulose, was then dissolved in 60 mL of KOH solution (24% w/v) taking advantage of the differences on cellulose and hemicellulose solubility in alkaline medium. After stirring for 15 h, the sample was filtered through a No. 1 crucible. The cake was then washed with deionized water until neutral pH was obtained at the filtrate, then with a dilute solution of CH_3COOH, and finally with ethanol. The cake corresponds to the

https://doi.org/10.1021/acs.biomac.3c00515
Biomacromolecules 2023, 24, 3872−3886

cellulose content, which was later dried and quantified. The hemicellulose content was then determined by difference.

2.5. Fourier-Transform Infrared Spectroscopy. The FTIR-attenuated total reflectance (FTIR-ATR) spectra were collected on a PerkinElmer Spectrum II spectrometer equipped with a diamond crystal plate ATR MIR single-reflection accessory, at a resolution of 4 cm^{-1} from 500 to 4000 cm^{-1}.

2.6. Water Retention Value. The water retention value (WRV) of the fibers was determined according to TAPPI UM256 (TAPPI 2011). In detail, approx. 1.5 g (o.d.w.) of pulp was placed in a centrifuge at 3000 G-force for 30 min to remove all free water. The centrifuged cellulosic samples were weighed before and after oven drying at 105 °C to determine WRV referring to the difference between the wet weight after centrifugation (w_{wet}) and the dry weight after oven drying (w_{dry}) to the dry weight, as detailed in eq 4.

$$\text{WRV}\ (\%) = \frac{W_{wet} - W_{dry}}{W_{dry}} \times 100 \quad (4)$$

An average WRV value was calculated from triplicates.

2.7. Carboxyl Content. The carboxyl content (CC) was determined by conductometric titration on the fibers prior to high-pressure homogenization in a Meter Basic 30 (Crison Instruments, S.A., Spain), as reported in previous studies.[35] The experiment was carried out taking 100 mg of fibers suspended in 15 mL of a 0.01 N HCl solution and kept under gentle stirring for 10 min. During this period, Na^+ cations are expected to be exchanged by protons H^+. The suspension was then titrated by adding a 0.01 N NaOH solution, while recording the conductivity for each 0.1 mL of NaOH addition. The titration curve exhibited the presence of a strong acid (excess of HCl) and a weak acid (carboxylic acid). The CC was then calculated according to eq 5.

$$\text{CC} = 162 \times (V_2 - V_1) \times c \times [w - 36 \times (V_2 - V_1)] \quad (5)$$

where V_1 and V_2 are the equivalent volumes of NaOH, in liters, c is the concentration of NaOH (0.01 M), w is the dry weight of the sample, in grams, 162 is the molecular weight of unsubstituted anhydroglucose (AGU), and 36 refers to the difference between the molecular weight of the substituted carboxylate form of AGU (198 g mol^{-1}) and that of the unsubstituted AGU (162 g mol^{-1}).[36]

2.8. Yield in Lignocellulosic Material. The yield in lignocellulosic material was determined by weight difference (based on dry weight) between the initial biomass weight and the recovered fibers after the hydrothermal treatment, filtration, and washing process.

2.9. Transmission Electron Microscopy of LCNFs. Droplets of dilute LCNF suspensions were deposited onto glow-discharged carbon-coated copper grids and stained with 2 wt % uranyl acetate. The specimens were observed using a JEOL JEM 2100-Plus microscope operating at 200 kV. Images were recorded on a Gatan Rio 16 camera.

2.10. Degree of Polymerization. The degree of polymerization (DP) was measured by the standard method for cellulose, TAPPI T236. Briefly, dried fibers (0.15 to 0.05 g) were dissolved in 0.5 M copper ethylenediamine (CED) (20 mL). Intrinsic viscosities of the solutions were obtained by using a Cannon-Fenske capillary viscometer, and the DP was calculated from the Mark–Houwink–Sakurada equation, $DP^{0.905} = 0.75\ [\eta]$. A dissolution time between 1 and 2 days was necessary to ensure complete dissolution of the fibers. However, for neat DPW and fibers with lignin content exceeding 15 wt %, a delignification step using sodium chlorite ($NaClO_2$), which can be delignified selectively and does not degrade the fibers, was required. For this, 0.6 g of $NaClO_2$ and 1 mL of glacial CH_3COOH were added per gram of fiber, previously dispersed in 50 mL of water. The suspension was then stirred at 70 °C for 1 h until the fibers turned into white and were well individualized.

2.11. Particle Size and ζ-Potential Measurements. The particle size and surface charge were measured at 25 °C by dynamic light scattering (DLS) using a Zetasizer ZS apparatus from Malvern. The concentration of the LCNF suspension was kept at around 0.2 wt % and pH-controlled by NaOH/HCl (10^{-3} M). Each measurement was performed in triplicate.

2.12. Rheological Measurements. The rheological measurements were carried out at 25 °C, using a stress-controlled rheometer (Kinexus Pro+, Malvern Instruments, U.K.) with a cone plate geometry (cone angle, 2°; diameter, 20 mm; truncation, 56 μm). Dynamic mode tests were performed by first measuring the storage modulus G' and the loss modulus G'' vs strain to determine the linear behavior domain. Then, a frequency sweep at a fixed strain in the linear domain was performed.

2.13. Nanopaper Production. Nanopapers were prepared by vacuum filtration of LCNF suspensions at a consistency of around 0.2 wt % using a Rapid-Köthen sheet former equipped with a 0.22 μm nitrocellulose filter membrane to retain all nanoscale elements of the LCNF suspension. The suspension was left to dewater until a gel-like cake of LCNFs was obtained on top of the membrane. The membranes were then vacuum-dried for 20 min and finally conditioned in a climate chamber at 23 °C and 50% of relative humidity for 24 h before testing.[37]

2.14. Nanopaper Characterization. Nanopapers were mechanically tested in an Instron universal testing machine provided with a 2.5 kN load cell. The gap between the clamps was set at 150 mm and the preload was 0.1 N with a cross-head testing velocity of 15 mm min^{-1}. The testing specimens were cut down to180-mm-long and 15-mm-wide stripes.

Transmittance measurements were performed on nanopapers, introducing the samples in a UV–visible (UV–vis) spectrophotometer without cuvettes. The wavelength was ranged between 400 and 800 nm, using air as reference.

Water contact angles on the nanopaper surface were measured using a DSSA25 drop-shape analyzer from Krüss GmbH (Germany) with Krüss Advance Software. The measurements were performed at room temperature with a frequency of two measurements per second. The total testing time was 10 min for each nanopaper.

X-ray diffraction (XRD) patterns were recorded in vacuum from strips of nanopapers using the Ni-filtered Cu Kα radiation (λ = 0.15418 nm) produced with a Philips PW3630 generator operating at 30 mV and 20 mA. Two-dimensional diffraction patterns were recorded on Fujifilm imaging plates read with a Fujifilm BAS 1800II bioanalyzer. Diffraction profiles were calculated as rotational averages of the two-dimensional (2D) patterns and normalized to the total amount of material by integrating the profile area between 7 and 37°.

In order to observe the film surface, strips were fixed flat on metallic stubs with carbon tape. To observe the cross section of the films, strips were fractured in liquid nitrogen and fixed end-on on the metallic stub. All samples were sputter-coated with Au/Pd and observed in secondary electron mode in a Thermo Scientific Quanta 250 field-emission scanning electron microscope (FE-SEM) operating at an accelerating voltage of 2.5 kV.

The thermal behavior of the nanopapers was analyzed to evaluate the thermal stability of fibers, using about 10 mg of solid samples and a PerkinElmer Pyris thermogravimetric analyzer from 20 to 600 °C, at a heating rate of 10 °C min^{-1}, under an oxygen atmosphere.

3. RESULTS AND DISCUSSION

3.1. Effect of HTT and MA Treatments over DPW. Figure 1 shows the chemical composition (A), the FTIR spectra (B), and the yield of the pretreatment, CC, and DP (C) of the neat DPW, the HTT-treated DPW (DPW-HTT), and the MA-treated DPW fibers.

The neat DPW exhibited cellulose, hemicellulose and lignin contents of 44, 22 and 28 wt %, respectively, indicating that ashes and extractives represented a residual fraction of the lignocellulosic feedstock (6 and 3 wt %, respectively). The HTT treatment favored the partial dissolution of hemicelluloses, with a decrease from 22 to 17 wt %, and lignin from 28 to 26 wt %, with no apparent effect over the cellulose content, which was increased from 44 to 52 wt %, (Figure 1A).

https://doi.org/10.1021/acs.biomac.3c00515
Biomacromolecules 2023, 24, 3872–3886

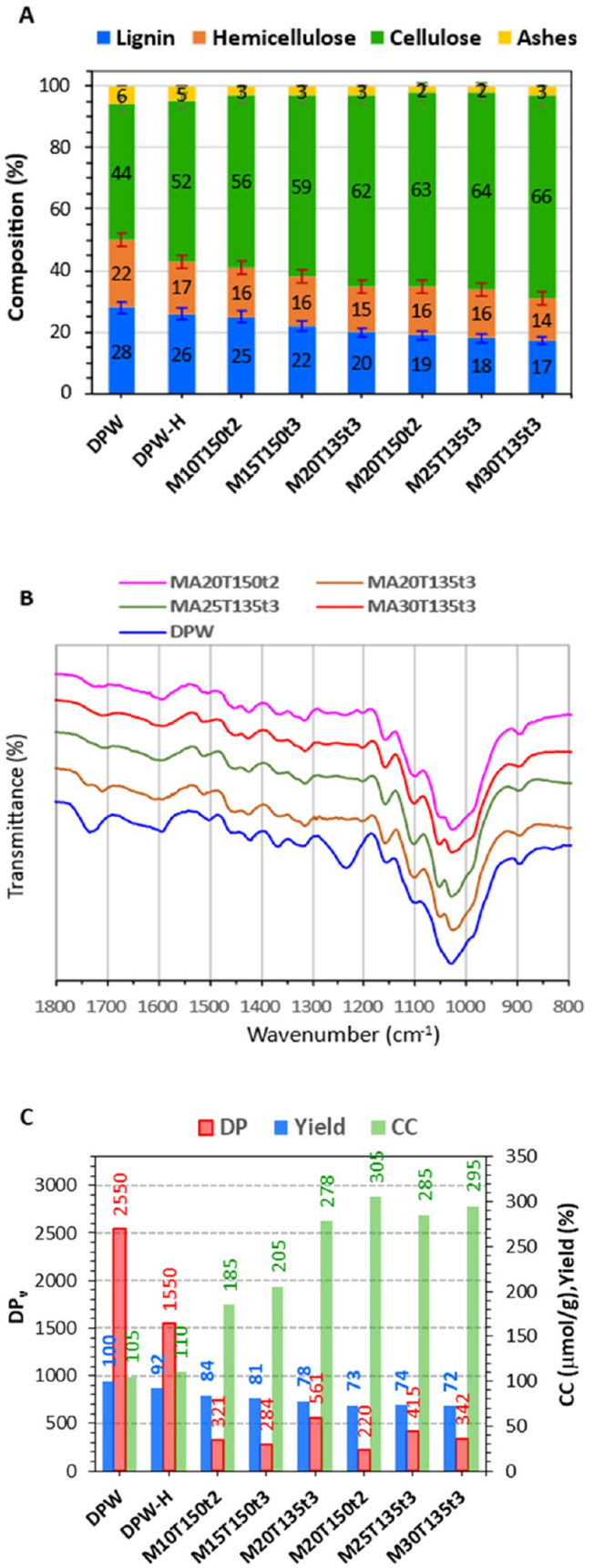

Figure 1. Chemical composition (A), FTIR spectra (B), and (C) DP (values in red), CC (values in green), and yield of the pretreatment (values in blue) (C) of the lignocellulosic fibers from DPW after different hydrothermal treatments.

On the contrary, the MA treatment significantly modified the lignin content of the DPW fibers. For example, the sample M30T135t3 experienced a reduction on lignin content from 28 to 14 wt %, hemicelluloses decreased from 22 to 14 wt %, while cellulose content represented a higher fraction, from 44 to 66 wt %. With the increase in the temperature and the residence time, the solubilization of hemicelluloses and lignin became more remarkable. These results agree with literature data, where the HTT treatment of lignocellulosic fibers at a temperature below 180 °C affected mainly the hemicellulose content,[39] which is the most sensitive to hydrolysis. Indeed, other HTT treatments, such as steam explosion (SE), have been reported to successfully solubilize and depolymerize hemicellulose, while having a milder effect over cellulose and lignin.[40,41] In addition, the more severe effect over hemicellulose and lignin fractions due to the presence of MA has been also reported, particularly for MA concentrations exceeding 50 wt % and high temperatures.[42] Considering the main objective of the present work, i.e., preserving the lignin content as much as possible during the conversion of DPW into LCNFs, the highest temperature of the experimental batch was set at 150 °C and the MA concentration at a maximum of 30 wt %. However, these maximum conditions were never set simultaneously, limiting the MA concentration to 20 wt % and 2 h, except for the case of 15 wt %, where treatment time was set at 3 h. The reagent concentration was increased to 30 wt % for 3 h only in the case of the 135 °C MA treatment. The obtained FTIR spectra of the solid fractions after different MA treatments exhibited the main bands originating from cellulose, hemicellulose, and lignin (Figure 1B). The main cellulose bands were visible at 898 cm^{-1} (C−H deformation vibrations), 1020 and 1052 cm^{-1} (C−O stretching), 1110 and 1157 cm^{-1} (C−O−C ring-stretching vibration), 1202 and 1230 cm^{-1} (C−OH in plane bending), 1265 cm^{-1} (C−H bending), 1314 cm^{-1} ($C-H_2$ wagging), 1332 cm^{-1} (C−OH in plane bending), 1366 cm^{-1} (C−H bending), and 1421 cm^{-1} ($C-H_2$ symmetric bending). The main hemicellulose bands appeared at 1455 cm^{-1} (C−H bending), 1600 cm^{-1} (COO− asymmetric stretching), and 1740 cm^{-1} (C═O stretching).[43] The lignin bands were visible at 1328 cm^{-1} (guaiacyl-syringyl-ring), 1503 cm^{-1} (aromatic skeletal vibrations), 1591 cm^{-1} (aromatic skeletal vibrations and C═O stretching), and 1705 cm^{-1} (C═O stretching in unconjugated ketones, conjugated aldehydes, and carboxylic acids).[44] In the neat DPW, in addition to cellulose, hemicellulose, and lignin bands, strong bands at 1235 and 1735 cm^{-1} were observed which could have likely originated from extractives and pectin. The persistence of the main FTIR bands of cellulose, hemicelluloses, and lignin in different samples further confirmed that during the MA treatment, at a concentration below 30 wt %, a low temperature (below 150 °C), and limiting the treatment time to less than 3 h, all of these constituents remained on the lignocellulosic fibers. Referring to the work of Su et al.,[42] the effect of MA treatment over wheat straw at 120 °C, 60 wt % of MA, and during 60 min led to the removal of about 75 and 56 wt % of hemicelluloses and lignin, respectively, resulting in fibers with hemicellulose and lignin contents around 8 and 16 wt %, respectively.

The degree of polymerization of the fibers was also measured to assess how the different treatments affected the fibers, and indirectly indicate a degradation of the lignocellulosic constituents. The DP was estimated using viscosimetry measurement in CED solution. Since the presence of lignin

https://doi.org/10.1021/acs.biomac.3c00515
Biomacromolecules 2023, 24, 3872−3886

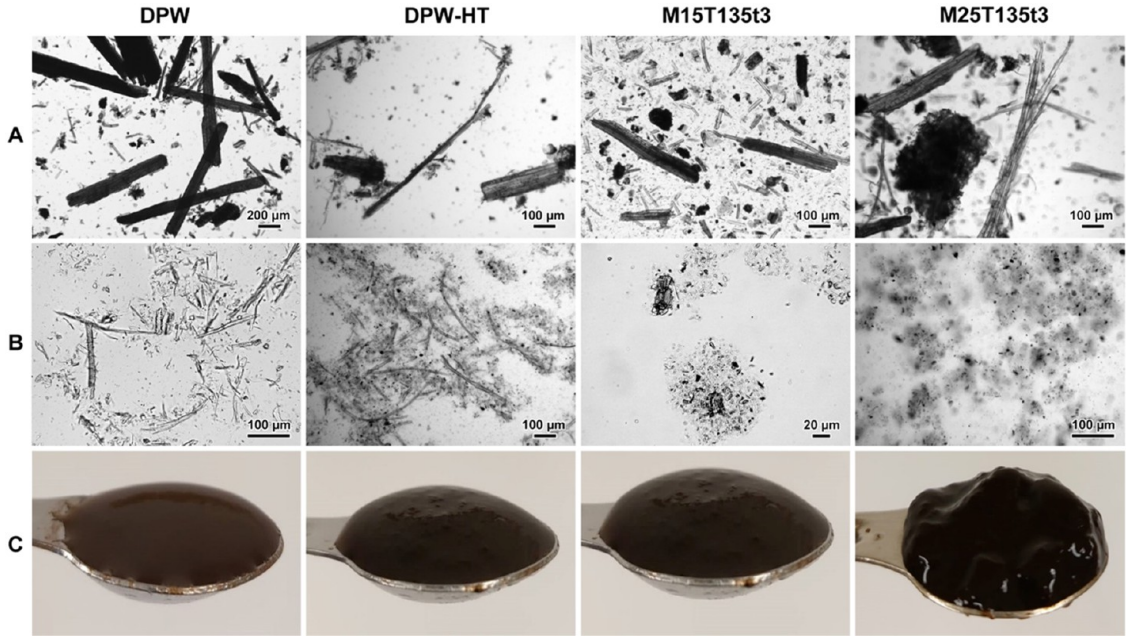

Figure 2. (A, B) Optical micrographs of DPW after different treatments: (A) HTT and MA treatments and (B) high-pressure homogenization. (C) Visual aspect of the LCNF gel at 1 wt % solid content.

hampers the dissolution of cellulose and might affect the measurement, a delignification treatment using sodium chlorite ($NaClO_2$) was performed, which selectively removes lignin, with low effect on the DP of cellulose, and no solubilization of glucan and hemicelluloses, mainly due to the lower effect over the pH of $NaClO_2$ compared to other oxidants, such as NaClO.[45] The results reported in Figure 1C indicate a significant decrease in DP after the HTT treatment, being the effect more pronounced when the HT-treated DPW was subjected to MA treatments. The DP of the neat DPW was found to be around 2500 and dropped to about 1500 after the HTT at 160 °C for 3 h. The decrease in DP was expected and in line with the literature data. Under the HTT, the hot compressed water accesses the inner structures of cellulosic biomass and induces bond cleaving and depolymerization of the cellulose backbone.[46] In the presence of MA, the magnitude of the DP decrease was much more pronounced and favored at increasing MA concentration and temperature. For instance, for the sample treated in the presence of 20% MA and a 135 °C during 3 h (M20T135t3), the DP reached 561 and decreased to 342 when the concentration of MA increases to 30 wt % (M30T135t3). The temperature of the biomass treatment also markedly affected the DP, which decreased from 651 to 284 when the biomass treatment was carried out with 20% MA and at 135 °C (M20T135t3) and 150 °C (M20T150t2), respectively. The higher DP decrease in the presence of MA is presumably due to the acidity brought by MA which is known to catalyze the cleavage of the glycosidic bonds. The yield in SF after the HTT achieved a high value around 92% when the pretreatment was run in the absence of MA, and dropped to 70−80% in the presence of MA. The increase in MA concentration during the HTT contributed to decrease in the yield, which is likely due to the removal and solubilization of hemicelluloses and lignin.

After the MA treatment, the carboxyl content also increased from about 100 μmol g^{-1} for the neat DPW to around 200−300 μmol g^{-1} depending on the conditions of the MA treatment (Figure 1C). CC was the highest for M20T150t2 (305 μmol g^{-1}) and the lowest for M10T150t2 (185 μmol g^{-1}). However, in comparison with other chemical pretreatments such as TEMPO-mediated oxidation or carboxymethylation,[19,37,47] these CC values are lower. We presumed that carboxylic groups originated from the esterification reaction of MA with hydroxyl groups of hemicelluloses and cellulose, leaving the second carboxyl group of MA on the fibril surface. Given the reversibility of the esterification reaction and its relatively low equilibrium constant (between 0.5 and 1), a low esterification fraction of hydroxyl groups of DPW by MA is expected. This justifies the low CC of the MA-treated DPW, but also the increase of CC with MA concentration.

The HTT also affected the WRV of the fibers in relation to the capacity of fibers to swell and accumulate water within the internal pores. As shown in Figure S1, the WRV significantly increased by more than 200% after the HTT in the presence of MA, while in the absence of MA, only a moderate increment in WRV of about 38% was noted after the HTT. This indicates an increase in water accessibility into the internal pores and interstices of fibers when the HTT was performed in the presence of MA.

3.2. LCNFs from DPW. LCNFs were prepared by HPH, with three passes at 300 bar followed by additional three passes at 600 bar at a solid content (SC) of around 1.5 wt %. These conditions are not harsh and are commonly adopted in the preparation of CNFs starting from chemically pretreated cellulose fibers.[17] The same procedure was adopted for all samples, making the pretreatment conditions of all LCNFs comparable. We collected images of the resulting LCNF gels at the same solid content (Figure 2). Except for the suspension from neat DPW fibers, which remained fluid after HPH, the other samples exhibited an intense brown color, together with a gel-like aspect at a solid content of 1.5 wt %. In the absence of MA, or at a concentration of MA below 15 wt %, the LCNF suspensions were fluid. The optical micrographs of the M15T150t3 LCNFs revealed the presence of residual fiber

https://doi.org/10.1021/acs.biomac.3c00515
Biomacromolecules 2023, 24, 3872−3886

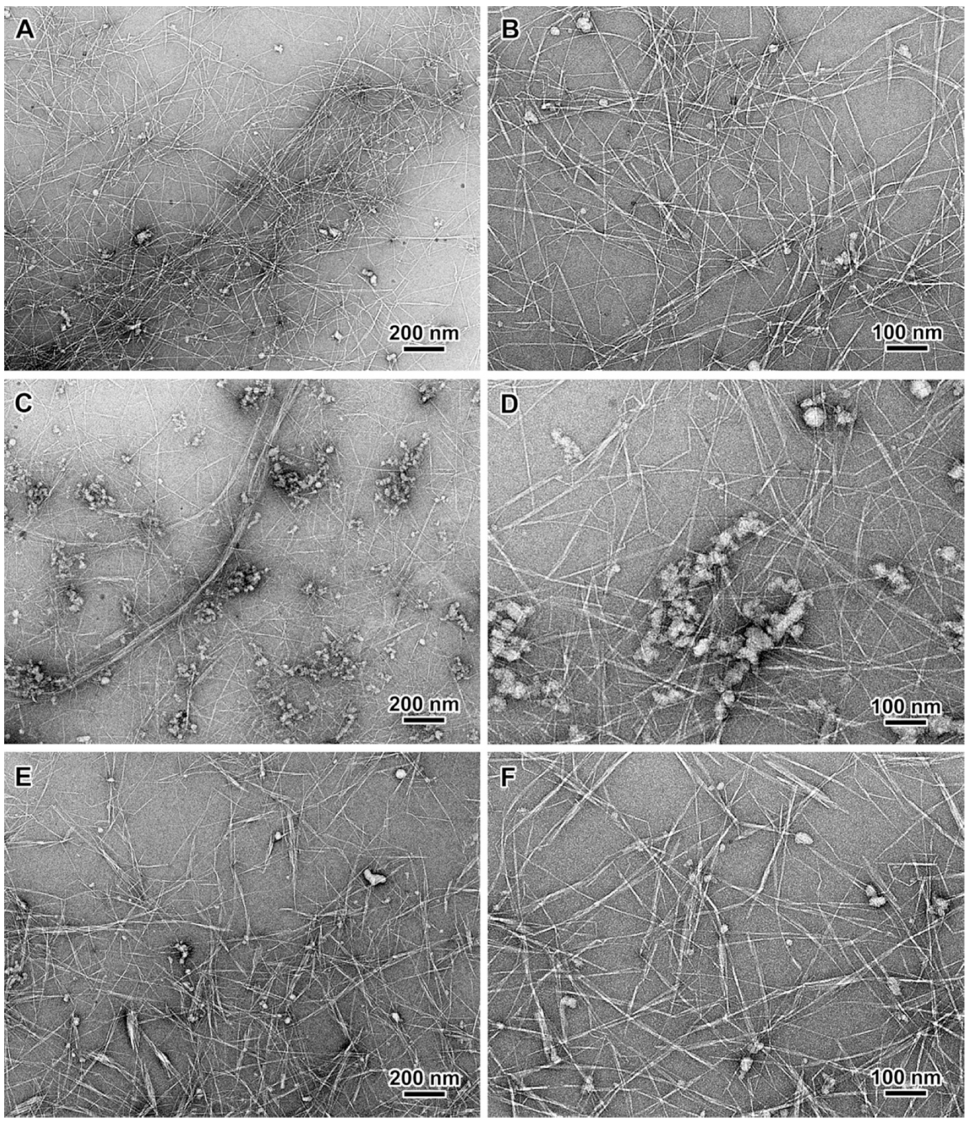

Figure 3. TEM images of negatively stained preparations from dilute suspensions of M20T135t3 (A, B), M30T135t2 (C, D), and M20T150t2 (E, F) LCNFs.

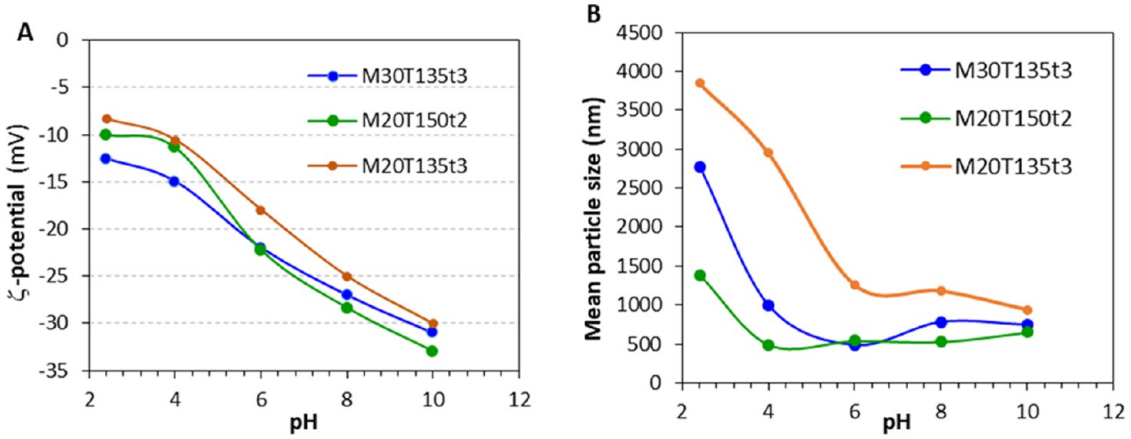

Figure 4. Colloidal properties of LCNFs from DPW: (A) ζ-potential *vs* pH, (B) mean particle size, and (C) size distribution at different pH.

fragments after HPH, which is indicative of a poor fibrillation extent of the treated fibers (Figure 2). However, the fraction of residual microsized fibers was lower than that in the case of DPW-HTT, confirming the beneficial effect of MA in promoting the breakdown of the lignocellulosic fibers (Figure 2). Over a concentration of 20 wt % of MA, and at a HTT temperature exceeding 135 °C, samples M25T135t3 and M20T150t2 did not contain any visible fragments of residual

https://doi.org/10.1021/acs.biomac.3c00515
Biomacromolecules 2023, 24, 3872−3886

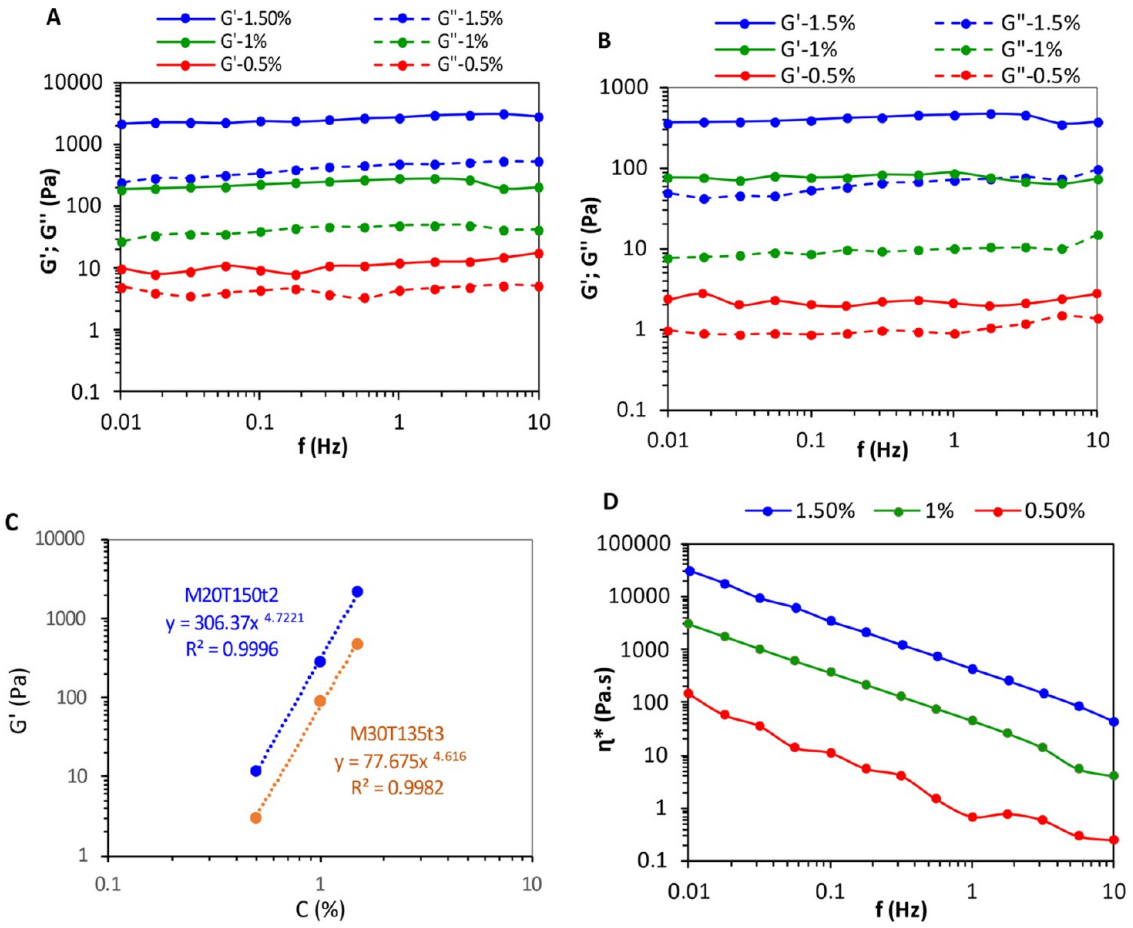

Figure 5. Rheological analysis of the LCNF gel: (A) Frequency sweeps of G' and G'' for LCNFs from M20T150t2 and (B) M30T135t3 at different solid contents (1.5, 1.0, and 0.5 wt %), (C) storage modulus G' at 1 Hz vs solid content. The dashed lines correspond to the fit of the power law $G' = KC^n$ on experimental measurements. (D) Corresponding complex viscosity.

fibers, with only sporadic brown spots, which indicates the effective fibrillation of the pretreated fibers after HPH.

The TEM images of the three types of LCNFs in dilute suspensions revealed individual or bundled nanofibrils that were generally kinked and formed entangled networks (Figure 3). It is worth pointing out that for M20T150t2, many shorter bundles (with a typical CNC length) could be seen, in agreement with the lower DP achieved when the MA treatment was performed at 150 °C (Figure 1C) The length of individual cellulose nanofibrils exceeded 1 μm, while their width ranged from 3 to 5 nm (Figure S2). Spheroidal 20−50-nm-large nanoparticles were also observed, as well as larger aggregates. They may correspond to lignin released from the fiber surface during HPH treatment in the form of nanoparticles or correspond to the precipitation of dissolved lignin after the MA treatment at a temperature exceeding 100 °C. The presence of such spherical particles at the surface of the fibrils has been previously observed by other authors, and the effect of HPH over the lignin content during fibrillation has been reported to decrease.[16,41,48] The lignin nanoparticles (NPs) appeared to be well distributed within the nanocellulose networks. It is worth mentioning that a fraction of free lignin NPs was also present in the supernatant recovered by filtration of the HTT-treated biomass (Figure S3).

The colloidal properties of the LCNF suspensions were studied by ζ-potential measurement and particle size distribution analysis at different pH, using DLS. For the three LCNF samples, prepared at temperatures of 135 and 150 °C, and MA concentration of 20 and 30 wt % for 2 and 3 h, the ζ-potential was negative over a pH range 4−10, with an absolute value exceeding 20 mV over pH 7, indicating the presence of negatively charged particles in this pH domain (Figure 4A). As the ζ-potential decreased, in absolute value with the pH, these negative surface charges were attributed to carboxyl groups originating from residual hemicelluloses and grafted MA through esterification with hydroxyl groups of cellulose and lignin. The amplification of hydroxyl groups for the MA-treated fibers, previously observed in the FTIR analysis, supports this hypothesis. The LCNF particle size distribution at different pH is shown in Figure 4B. This analysis was used mainly to assess the evolution of the colloidal stability of the LCNF particles with pH, rather than to estimate the size of fibrils, as the DLS analysis provides a measurement the hydrodynamic diameter of a sphere with an equivalent translational diffusion coefficient.[49] At decreasing pH, the mean particle size increased, indicating the occurrence of aggregation. The same tendency was observed for the three LCNF samples prepared under different conditions. This effect, whose magnitude became pronounced at pH 3, is due to the decrease in the ionization degree of the carboxyl group with pH reduction, leading to a reduction of the ζ-potential of the particles and consequently a reduction of the electrostatic barrier. This can be seen in Figure S4, where an excessive

https://doi.org/10.1021/acs.biomac.3c00515
Biomacromolecules 2023, 24, 3872−3886

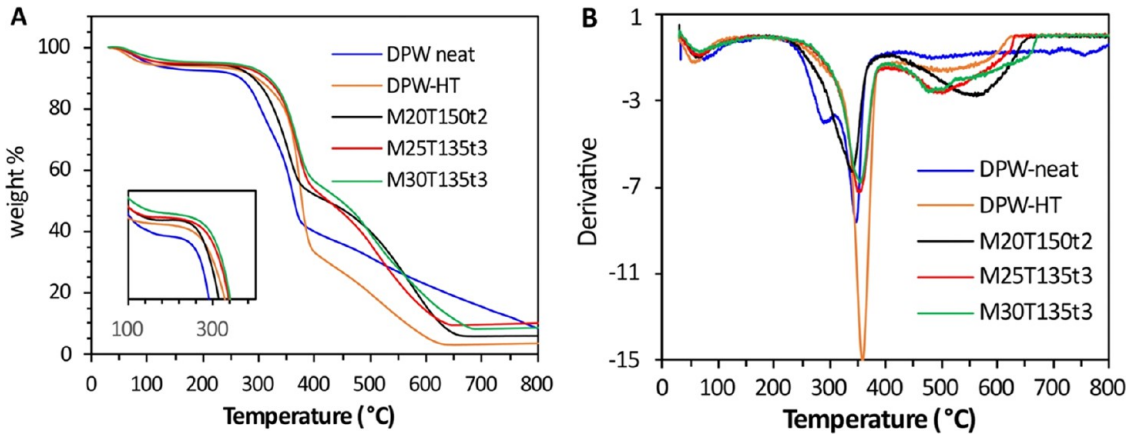

Figure 6. Thermogravimetric (A) and corresponding derivative thermogravimetric (DTG) (B) curves of the neat DPW, DPW-HT, and MA-treated samples.

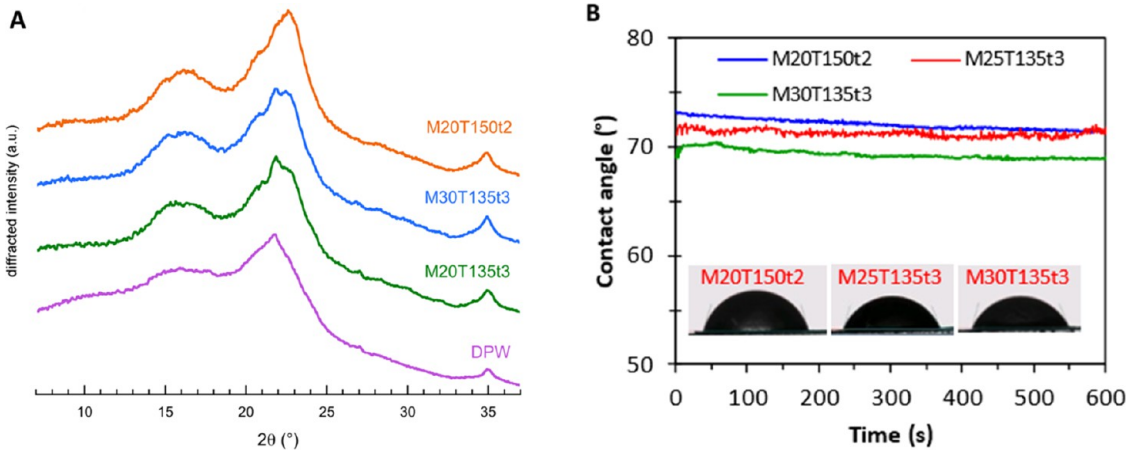

Figure 7. (A) X-ray diffraction profiles for DPW and LCNFs and (B) contact angle of water on LCNF films as a function of time.

aggregation of the LCNF particles spontaneously occurred as the pH was reduced to 2.

The rheological behavior of the LCNFs at different solid contents was investigated by oscillatory sweep measurements of the storage modulus (G') and loss modulus (G'') as a function of frequency (f) in the linear domain (Figure 5A,B). The measurement was performed for LCNFs from M20T150t2 and M30T135t3. At any of the tested solid contents (0.5−1.5 wt %), the LCNF suspensions exhibited a gel-like character, as confirmed by the higher magnitude of G' in comparison with G'' and by their frequency independence over the investigated frequency domain (0.01−10 Hz). The gel-like character is typical of CNF suspensions with a high degree of fibrillation (effective breakdown of cellulose fibers into nanofibrils) and is the result of the generation of entangled CNF networks, which are easily formed even at low solid content (SC < 0.5%) thanks to the high aspect ratio of the CNFs, their high flexibility, and high surface area, which directly correlates with their high capacity to retain water.[50,51] Thereby, the gel aspect of the LCNFs indicates an extensive fibrillation, as demonstrated by TEM observation. The presence of lignin NPs entrapped within the CNF network might also contribute to enhance the gel character of the LCNF suspension through possible lignin−lignin or lignin−fibril NP interaction. The dependence of G' with LCNF concentration (Figure 5C) revealed a power−law relationship ($G' = KC^n$) with a regression coefficient R^2 exceeding 0.99, which was found for different gels, where C is the weight concentration of LCNFs, and the K factor and n power are characteristic of the fibril characteristics and the structural property of the LCNF suspension, respectively. The exponent factors for both LCNF suspensions were around 4.5−4.7, which are higher than those obtained for CNFs (between 1.5 and 2.8).[52]

The thermal stability of the LCNFs was studied by thermogravimetric analysis (TGA) under air flow and compared to that of the neat DPW (Figure 6). The TGA curves of all samples exhibited a first weight loss of about 5 wt % at 90−100 °C associated with water removal, followed by a two-step weight loss from 250 to 600 °C, resulting from the thermal degradation of the main components in the biomass. The first weight loss results, presumably, from the degradation of hemicellulose and cellulose, which are the least sensitive to thermal degradation, followed by the thermal decomposition of lignin and the complete oxidative degradation of the carbonaceous residue formed during the first step. The onset of the thermal degradation was the lowest for neat DPW followed by DPW-HT, with an onset thermal degradation (T_{onset}) at 210 and 220 °C, respectively. The lower T_{onset} of neat DPW is presumably due to the presence of volatile extractives and higher content of hemicelluloses. The LCNFs exhibited a higher thermal stability with a T_{onset} exceeding 240

https://doi.org/10.1021/acs.biomac.3c00515
Biomacromolecules 2023, 24, 3872−3886

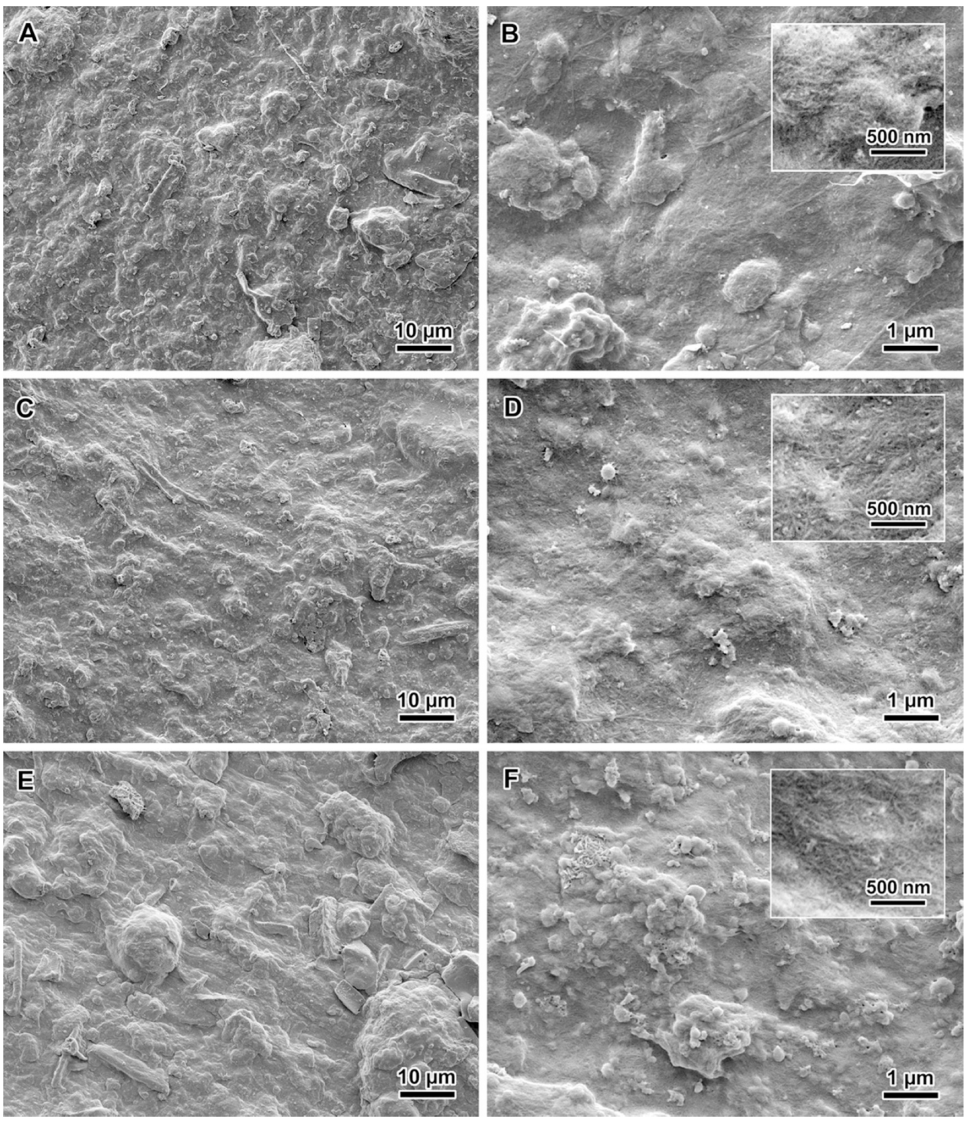

Figure 8. FE-SEM images of the surfaces of nanopapers from M20T135t3 (A, B), M30T135t3 (C, D), and M20T150t2 (E, F) LCNFs.

°C. Similar results were found in the literature for LCNFs with different lignin content produced by partial delignification using sodium chlorite and acetic acid treatment of thermo-mechanical pulp.[53] This better thermal stability of LCNFs is due to the presence of lignin, which starts to degrade over 400 °C. The higher residue from 600 °C can be attributed to the generation of a carbonaceous layer onto the MA-treated samples, as it has been previously found for other chemically modified CNFs.[37] Indeed, the weight fraction of the residue increased with the carboxyl content, which supports this hypothesis.

The XRD profiles of M20T135t3, M30T135t3, and M25T135t3 LCNFs are shown in Figure 7A. They exhibit diffraction peaks of cellulose I. According to the indexing of the Iβ allomorph, the broad peak at 2θ = 16.1° results from the overlapping of the $1\bar{1}0$ and 110 reflections, while the peaks at 22.5 and 34.9° correspond to the (200) and (004) crystal planes.[54] In addition to these features, the profile of DPW contains a peak at 21.8°. This reflection does not arise from cellulose and may result from the presence of crystalline epicuticular wax.[55] The fact that this peak also occurs in the profiles of M20T135t3 and M30T135t3 LCNFs means that this compound resisted the treatments with MA. However, it was absent in the treatment carried out at 150 °C (M20T150t2). The quantitative analysis of the XRD profiles is not straightforward since all samples contain various amounts of cellulose, lignin, and other constituents. In particular, Segal's method[38] to calculate a crystallinity index cannot be used directly since the specimens do not contain only cellulose. However, since the profiles were normalized to the total amount of the sample, it is clear that the crystalline fraction increases, which is consistent with the increase of the cellulose fraction due to the gradual removal of lignin and hemicelluloses that contributes to the amorphous background of the profiles.

One of the impacts of the presence of lignin in LCNFs is the reduction in the hydrophilic character of thin films produced by casting or vacuum filtration. To assess this property, thin films were prepared by vacuum filtration of dilute LCNF suspensions, and their dynamic water contact angle (WCA) was measured over a period of 10 min (Figure 7B). The data presented for M20T150t3, M25T135t3, and MA30T135t3 showed a nearly similar contact angle around 70° for the three films, remaining almost unchanged with time. This value is

https://doi.org/10.1021/acs.biomac.3c00515
Biomacromolecules 2023, 24, 3872−3886

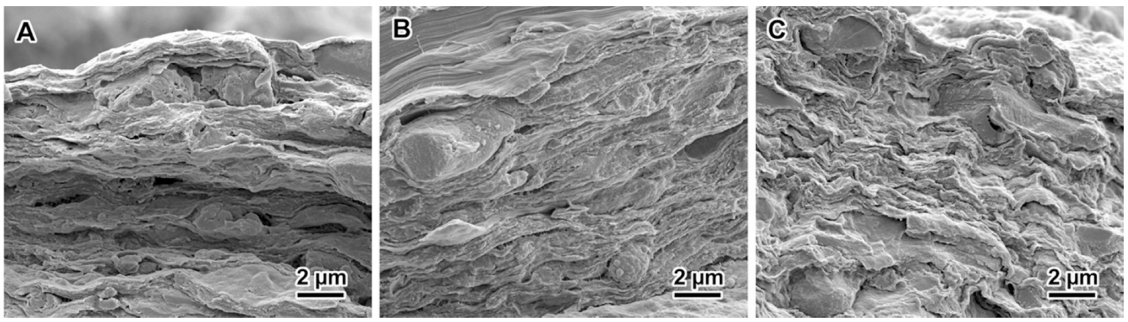

Figure 9. FE-SEM images of the cross sections of freeze-fractured nanopapers from M20T135t3 (A), M30T135t3 (B), and M20T150t2 (C) LCNFs.

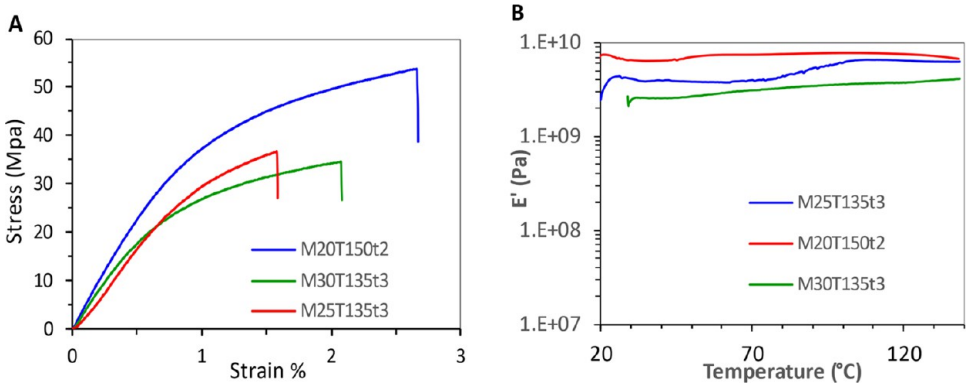

Figure 10. (A) Stress−strain curves and (B) DMA for thin nanopaper films from LCNFs.

much higher than those obtained for thin films from lignin-free CNFs, where a contact angle around 40−45° was typically reported.[52] Moreover, the stability of the WCA over time indicated that the drop of water was not absorbed by the film, even after 10 min. The relatively high contact angle observed for the LCNF films is explained by the presence of lignin NPs accumulated at the surface of the LCNFs, as confirmed by FE-SEM observations. These NPs are likely to accumulate on the surface of the film thanks to the spherical shape and to the hydrophobic properties of lignin. It is worth mentioning that the WCA values found in the present work agree with most of the literature data, where a contact angle between 70 and 90° has been reported, even when the lignin content was lower than 10 wt %.[48]

Nanopapers were prepared from the LCNF suspensions by vacuum filtration and their topography was analyzed by FE-SEM and the images revealed that the surfaces of the M20T135t3, M30T135t3, and M20T150t2 nanopapers had a granular aspect (Figures 8 and S5). The origin of this granularity cannot be determined from SEM images alone as high-magnification images clearly show that the film surface was covered with cellulose nanofibrils (insets in Figure 8B,D,F). Occasional residual fiber fragments were observed both on the surface and inside the films (Figures 8A,C,E and 9). As can be seen in the cross sections (Figure 9A−C), the films exhibit a layered structure similar to that typically observed in lignin-free CNF nanopapers, which is explained by the mechanism of formation of the nanopaper sheet involving the deposition of successive layers of CNFs.[56] The lignin NPs that were observed among CNFs on TEM images (Figures 3 and S2 and S3) are too small to be clearly detected on these FE-SEM images, and they were presumably trapped within the nanofibril network during the deposition of different layers.[57] Nevertheless, particles with a wide size distribution (typically from 100 nm to 10 μm) seen both at the surface and inside the films may correspond to lignin aggregates that would be too large to be detected by TEM observation of the supernatants of the LNCF suspensions.

The mechanical properties of the nanopapers were studied by tensile test and dynamic mechanical analysis (DMA). From Figure 10A, it can be seen that the stress−strain plot of the film changed according to the preparation conditions of the LCNFs. The best performance was achieved with the sample M20T150t2, with a tensile modulus (E)/strength (σ_r) of about 6 GPa/54 MPa, followed by M30T135t3 and M25T135t3 demonstrating E/σ_r values at 4 GPa/35 and 3.2 GPa/36 MPa, respectively. The values of E from the tensile test agreed with those established from the DMA analysis which are in the range of 3−6 GPa. From the DMA analysis, it can also be seen that the modulus remained nearly unchanged between 20 and 140 °C, indicating that the stiffness of the nanopapers was preserved even after lignin softening. However, the strength of the obtained nanopapers was lower than that of lignin-free CNF nanopapers, where E/σ_r values between 8 and 15 GPa/80−300 MPa have been reported in the literature.[56,58] In fact, numerous factors are known to affect the mechanical properties of nanopapers, including chemical composition, morphology of the nanofibrils (diameter and length), method of preparation of the nanopaper, DP, density of the nanopaper, and nanofibril orientation, among others.[57] It is worth mentioning that the literature on the effect of residual lignin in LCNF nanopapers diverges. Some authors reported the insensitivity of the strength and tensile modulus of nanopapers containing up to 14 wt % lignin, while others outlined a lower strength and modulus for nanopapers with a high lignin content (around 27 wt %).[59,60] This disparity is likely due to

https://doi.org/10.1021/acs.biomac.3c00515
Biomacromolecules 2023, 24, 3872−3886

Scheme 2. Schematic Illustration of the Mechanism of Formation of LCNFs by Hydrothermal Treatment in the Presence of MA Followed by HPH

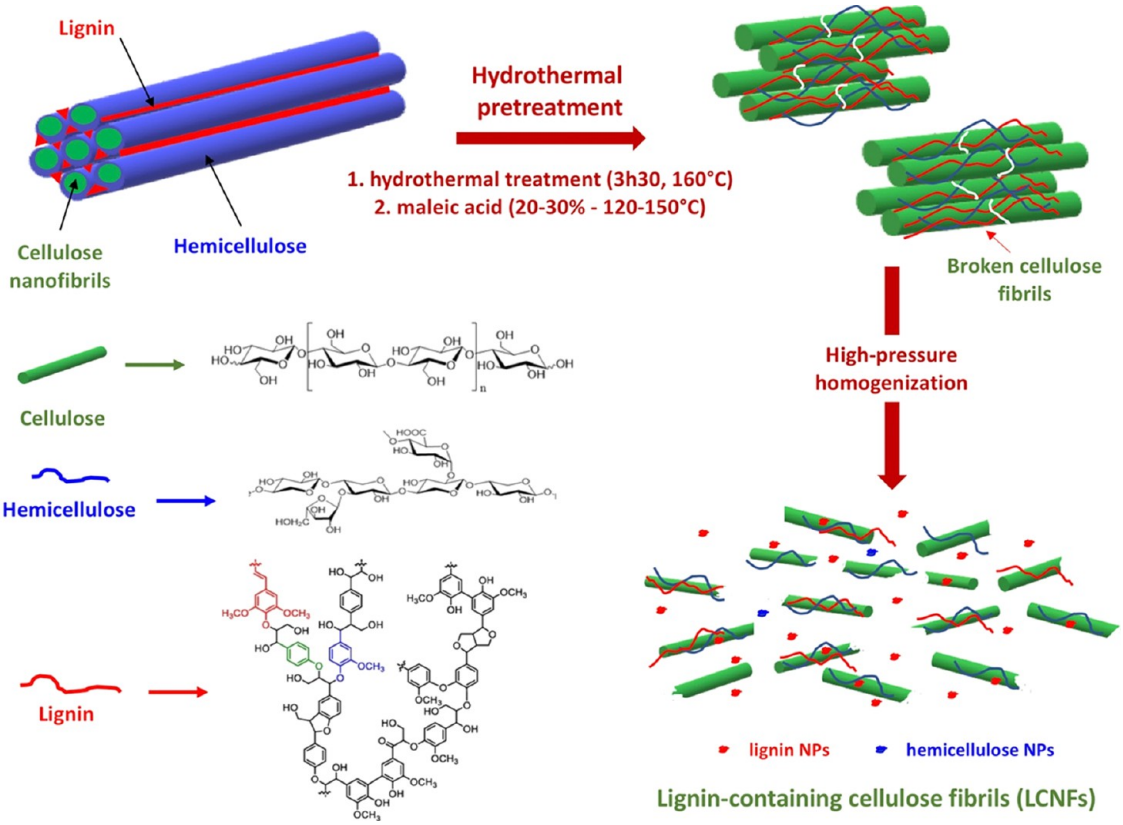

the difference in lignin content of the LCNFs. Presently, we ascribed the lower modulus and strength of the nanopapers to the relatively high content in lignin (over 20 wt %), which reduces the magnitude of hydrogen bonding between the entangled nanofibril network by interposing between them as shown in FE-SEM images of nanopaper cross sections. Since the strength of the nanopapers is mainly driven by the relative bonded area (RBA), any parameter likely to reduce the fibril−fibril bonding capacity inevitably results in a reduction in the strength of the nanopapers. The huge reduction in the DP of cellulose after the MA treatment is another parameter likely to reduce the strength of the nanopapers, mainly due to the unavoidable loss of aspect or slenderness ratio. The presence of microparticles originating from aggregated lignin or fragments of lignocellulosic particles could also contribute to the reduction in the strength of the film, by acting as a stress concentrator, from which fractures are initiated.

3.3. Mechanism of Disintegration of the Biomass. Based on the results from the present work, the following mechanism is proposed to explain the process of formation of LNCFs (Scheme 2). Under the combined effect of pressure, temperature, and MA, a fraction of lignin was removed either in the form of NPs or dissolved. This contributed to increasing the accessibility of the fibers as confirmed by the increase in the fiber WRV, favoring the expansion of the fibers and diffusion of water inside the fiber micropores. In addition, due to the acidity and temperature, a hydrolysis of glycosidic bonds occurred, as confirmed by the huge decrease in DP. The chain breaking is likely to occur mostly in the disorganized regions of the nanofibrils, thanks to their higher accessibility and lower cohesion than the crystalline domains. The combined effect of the DP decrease, fiber expansion, and lignin removal contributed to weakening the cohesion of the fibers and facilitated the breakdown of the biomass into their elementary components during the disintegration by HPH. The lignin was released in the form of NPs and the cellulose in the form of elementary bundles of nanofibrils. This hydrothermal pretreatment in the presence of MA is more or less similar to the chemical activation or pretreatment of the fibers via TEMPO-mediated oxidation, or periodate oxidation, where the chemical action contributed to reducing the cohesion degree among the elementary fibrils, which facilitated the breakdown of the cell wall under the effect of ultrasonication or high mechanical shearing effect.

Although several papers have reported the use of MA in biomass treatment and nanocellulose production, the present work differs in many aspects from what has been published so far.[28−33] Previous studies mainly focused on the use of MA as a hydrotrope to rapidly fractionate biomass at atmospheric pressure and low temperature, having as a main goal the separation and isolation of lignin from the plant cell wall by dissolution in the MA/water mixture. To achieve this, MA concentrations higher than 50% have been reported to be required to efficiently solubilize lignin through the aggregation of acid hydrotrope molecules. The acidity of MA also promotes the release of lignin by the catalyzed hydrolysis of ether and/or ester bonds in hemicelluloses and lignin carbohydrate complexes (LCCs). In contrast to previous studies, this work focused on converting neat biomass into nanoscale particles with the highest possible yield and minimum post-treatment, keeping MA below the minimum hydrotrope concentration (MHC), which is around 25%.[28] At

https://doi.org/10.1021/acs.biomac.3c00515
Biomacromolecules 2023, 24, 3872−3886

selected conditions, a significant fraction of lignin remained bound to the biomass, albeit with weaker interactions compared to the original biomass. As a consequence, the resulting LCNF suspension obtained after the disintegration process still contained a high lignin fraction, which is highly desirable for taking advantage of the benefits of lignin. It is estimated that over 75% of lignin remained in the LCNFs, whereas in previous works, over 55% of lignin was dissolved and removed from the fibers.

The treatment in the present study was performed at higher temperatures and under pressure (between 130−150 °C and 300−500 kPa) using hydrothermal conditions. This generated a synergistic effect for the breakdown of plant cell walls by increasing the expansion degree of the fibers and cleaving the LCCs in the disorganized regions. In addition, a mechanism explaining how the hydrothermal treatment in the presence of MA facilitates the breakdown of plant cell walls into nanofibrils and lignin NPs has been provided. The reduction in the degree of polymerization (DP) of cellulose fibrils and the expansion of fibers were identified as key parameters making the disintegration of treated biomass into nanoscale lignocellulosic material easier, which had not been reported previously.

Notably, without the hydrothermal treatment under appropriate conditions, it would have been impossible to turn the biomass into a thick gel. This represents a novelty and an original approach for converting neat biomass into nanoscale lignocellulosic material, including cellulose nanofibrils, lignin NPs, and other components. Furthermore, it is worth mentioning that the gel was obtained after only two passes through the high-pressure homogenizer. After six passes at a pressure lower than 500 bar, the thick gel remained stable without syneresis even after storage for more than 3 months at room temperature.

Regarding the potential uses of LCNFs, the high lignin content broadens their field of application, particularly in areas where the presence of lignin is desirable. Ongoing work is focused on utilizing the present LCNFs as a binder in particleboard fabrication, replacing urea-formaldehyde adhesive, but other applications such as food packaging are being explored. The presence of lignin contributes to an adhesive effect and improves water resistance due to lignin's hydrophobic character, which is of utmost importance in several sectors, such as fiberboards, but also fiber-based packaging.

4. CONCLUSIONS

In this work, the use of maleic acid (MA) at high temperature was proposed as a pretreatment of date palm waste (DPW) fibers for the production of lignocellulosic nanofibrils (LCNFs). The use of this MA-assisted treatment contributed to the preservation of lignin, minimizing the waste generated during the LCNF production compared to other chemical pretreatments for nanocellulose production, while providing unique properties to the LCNF gel. The carboxyl content (CC) was found to increase with the severity of the MA treatment, which resulted in long and entangled cellulose nanofibrils containing lignin (21−25 wt %). The resulting LCNFs exhibited a higher thermal stability when compared to LCNFs prepared in the absence of MA, increasing the onset temperature from 220 to 250−260 °C. These characteristics revealed the potential of MA-treated LCNFs for the production of nanopapers which exhibited a tensile strength of up to 54 MPa and a Young modulus of 6 GPa. In addition, the water contact angle (WCA) revealed the lower hydrophilicity of these films compared to lignin-free CNF nanopapers, as they were able to maintain a WCA of 70° for 10 min without drop absorption. Overall, the present work proposes an interesting method for producing high-lignin content LCNFs with unique properties and a high preservation of the starting material by comparison with other chemistry-based nanocellulose production strategies.

■ ASSOCIATED CONTENT

Data Availability Statement

Authors can make available the data used in this work upon request.

Supporting Information

The Supporting Information is available free of charge at https://pubs.acs.org/doi/10.1021/acs.biomac.3c00515.

Carboxyl content and water retention values of the LCNFs; high-magnification TEM images of negatively stained preparations from dilute suspensions of LCNFs and the suspension recovered after filtration of the M20T150t2 DPW fibers; images of the visual aspect of the LCNF suspensions at different pH values; the visual aspect of the LCNF films, and low-magnification SEM images of the LCNF films (PDF)

■ AUTHOR INFORMATION

Corresponding Authors

Marc Delgado-Aguilar − *LEPAMAP-PRODIS Research Group, University of Girona, 17003 Girona, Spain*; Email: m.delgado@udg.edu

Sami Boufi − *University of Sfax, LMSE, Faculty of Science, 3018 Sfax, Tunisia*; orcid.org/0000-0002-3153-0288; Email: sami.boufi@fss.rnu.tn

Authors

Amira Najahi − *University of Sfax, LMSE, Faculty of Science, 3018 Sfax, Tunisia*; orcid.org/0000-0001-7547-3281

Quim Tarrés − *LEPAMAP-PRODIS Research Group, University of Girona, 17003 Girona, Spain*; orcid.org/0000-0002-7021-2055

Jean-Luc Putaux − *Univ. Grenoble Alpes, CNRS, CERMAV, F-38000 Grenoble, France*; orcid.org/0000-0002-9760-5369

Complete contact information is available at: https://pubs.acs.org/10.1021/acs.biomac.3c00515

Author Contributions

A.N.: investigation, methodology; Q.T.: investigation, methodology; M.D.-A.: supervision, writing, review & editing; J.-L.P.: methodology, review & editing; S.B.: investigation, writing, review & editing

Funding

This work has been funded by the Spanish Ministry of Science and Innovation, project NextPack (PID2021-124766OA-I00), the Tunisian Ministry of Higher Education and Research, project 21P2ES-D6P3, and the Erasmus+ KA107 Program for the mobility grant of Amira Najahi.

Notes

The authors declare no competing financial interest.

■ ACKNOWLEDGMENTS

The authors wish to acknowledge the financial support of the funding agencies listed in the Funding section. A.N. is grateful for the funding from Erasmus for developing her internship at Universitat de Girona. M.D.-A. and Q.T. are Serra Húnter Fellows. The authors thank the NanoBio-ICMG Platform (UAR 2607, Grenoble) for granting access to the electron microscopy facility and Christine Lancelon-Pin (CERMAV) for SEM observations.

■ REFERENCES

(1) Kwon, G.-J.; Cho, S.-W.; Bandi, R.; Yang, B.-S.; Dadigala, R.; Han, S.-Y.; Ma, S.-Y.; Kim, J.-K.; Kim, N.-H.; Lee, S.-H. Production of Lignocellulose Nanofibrils by Conventional and Microwave-Assisted Deep-Eutectic-Solvent Pretreatments: Mechanical, Antioxidant, and UV-Blocking Properties. *Cellulose* **2023**, *30*, 4277−4292.

(2) Trovagunta, R.; Zou, T.; Österberg, M.; Kelley, S. S.; Lavoine, N. Design Strategies, Properties and Applications of Cellulose Nanomaterials-Enhanced Products with Residual, Technical or Nanoscale Lignin—A Review. *Carbohydr. Polym.* **2021**, *254*, No. 117480.

(3) Rojo, E.; Peresin, M. S.; Sampson, W. W.; Hoeger, I. C.; Vartiainen, J.; Laine, J.; Rojas, O. J. Comprehensive Elucidation of the Effect of Residual Lignin on the Physical, Barrier, Mechanical and Surface Properties of Nanocellulose Films. *Green Chem.* **2015**, *17*, 1853−1866.

(4) Serra-Parareda, F.; Aguado, R.; Tarrés, Q.; Mutjé, P.; Delgado-Aguilar, M. Chemical-Free Production of Lignocellulosic Micro-and Nanofibers from High-Yield Pulps: Synergies, Performance, and Feasibility. *J. Cleaner Prod.* **2021**, *313*, No. 127914.

(5) Herrera, M.; Thitiwutthisakul, K.; Yang, X.; Rujitanaroj, P.; Rojas, R.; Berglund, L. Preparation and Evaluation of High-Lignin Content Cellulose Nanofibrils from Eucalyptus Pulp. *Cellulose* **2018**, *25*, 3121−3133.

(6) Guo, S.; Li, X.; Kuang, Y.; Liao, J.; Liu, K.; Li, J.; Mo, L.; He, S.; Zhu, W.; Song, J.; et al. Residual Lignin in Cellulose Nanofibrils Enhances the Interfacial Stabilization of Pickering Emulsions. *Carbohydr. Polym.* **2021**, *253*, No. 117223.

(7) Chihaoui, B.; Tarrés, Q.; Delgado-Aguilar, M.; Mutjé, P.; Boufi, S. Lignin-Containing Cellulose Fibrils as Reinforcement of Plasticized PLA Biocomposites Produced by Melt Processing Using PEG as a Carrier. *Ind. Crops Prod.* **2022**, *175*, No. 114287.

(8) Belgacem, C.; Tarres, Q.; Espinach, F. X.; Mutjé, P.; Boufi, S.; Delgado-Aguilar, M. High-Yield Lignocellulosic Fibers from Date Palm Biomass as Reinforcement in Polypropylene Composites: Effect of Fiber Treatment on Composite Properties. *Polymers* **2020**, *12*, No. 1423.

(9) Sundholm, J. *Mechanical Pulping*; Fapet Oy, 1999; Vol. *5*.

(10) Boufi, S.; Gandini, A. Triticale Crop Residue: A Cheap Material for High Performance Nanofibrillated Cellulose. *RSC Adv.* **2015**, *5*, 3141−3151.

(11) Espinosa, E.; Tarrés, Q.; Delgado-Aguilar, M.; González, I.; Mutjé, P.; Rodríguez, A. Suitability of Wheat Straw Semichemical Pulp for the Fabrication of Lignocellulosic Nanofibres and Their Application to Papermaking Slurries. *Cellulose* **2016**, *23*, 837−852.

(12) Li, X.; Ning, C.; Li, L.; Liu, W.; Ren, Q.; Hou, Q. Fabricating Lignin-Containing Cellulose Nanofibrils with Unique Properties from Agricultural Residues with Assistance of Deep Eutectic Solvents. *Carbohydr. Polym.* **2021**, *274*, No. 118650.

(13) Sjöström, E.; Westermark, U. Chemical Composition of Wood and Pulps: Basic Constituents and Their Distribution. In *Analytical Methods in Wood Chemistry, Pulping, and Papermaking*; Springer, 1999; pp 1−19.

(14) Yaku, F.; Yamada, Y.; Koshijima, T. Lignin Carbohydrate Complex Pt. II. Enzymic Degradation of Acidic Polysaccharide in Björkman LCC. *Holzforschung* **1976**, *30*, 148−156.

(15) Eriksson, Ö.; Goring, D. A. I.; Lindgren, B. O. Structural Studies on the Chemical Bonds between Lignins and Carbohydrates in Spruce Wood. *Wood Sci. Technol.* **1980**, *14*, 267−279.

(16) Serra-Parareda, F.; Tarrés, Q.; Pèlach, M. À.; Mutjé, P.; Balea, A.; Monte, M. C.; Negro, C.; Delgado-Aguilar, M. Monitoring Fibrillation in the Mechanical Production of Lignocellulosic Micro/Nano Fi Bers from Bleached Spruce Thermomechanical Pulp. *Int. J. Biol. Macromol.* **2021**, *178*, 354−362.

(17) Serra-Parareda, F.; Tarrés, Q.; Sanchez-Salvador, J. L.; Campano, C.; Pèlach, M. À.; Mutjé, P.; Negro, C.; Delgado-Aguilar, M. Tuning Morphology and Structure of Non-Woody Nanocellulose: Ranging between Nanofibers and Nanocrystals. *Ind. Crops Prod.* **2021**, *171*, No. 113877.

(18) Delgado-Aguilar, M.; González, I.; Tarrés, Q.; Pèlach, M. T. À.; Alcalà, M.; Mutjé, P. The Key Role of Lignin in the Production of Low-Cost Lignocellulosic Nanofibres for Papermaking Applications. *Ind. Crops Prod.* **2016**, *86*, 295−300.

(19) Isogai, A.; Saito, T.; Fukuzumi, H. TEMPO-Oxidized Cellulose Nanofiber. *Nanoscale* **2011**, *3*, 71−85.

(20) Wen, Y.; Yuan, Z.; Liu, X.; Qu, J.; Yang, S.; Wang, A.; Wang, C.; Wei, B.; Xu, J.; Ni, Y. Preparation and Characterization of Lignin-Containing Cellulose Nanofibril from Poplar High-Yield Pulp via TEMPO-Mediated Oxidation and Homogenization. *ACS Sustainable Chem. Eng.* **2019**, *7*, 6131−6139.

(21) Najahi, A.; Tarrés, Q.; Mutjé, P.; Delgado-Aguilar, M.; Putaux, J.-L.; Boufi, S. Lignin-Containing Cellulose Nanofibrils from TEMPO-Mediated Oxidation of Date Palm Waste: Preparation, Characterization, and Reinforcing Potential. *Nanomaterials* **2023**, *13*, No. 126.

(22) Ewulonu, C. M.; Liu, X.; Wu, M.; Huang, Y. Ultrasound-Assisted Mild Sulphuric Acid Ball Milling Preparation of Lignocellulose Nanofibers (LCNFs) from Sunflower Stalks (SFS). *Cellulose* **2019**, *26*, 4371−4389.

(23) Liu, X.; Li, Y.; Ewulonu, C. M.; Ralph, J.; Xu, F.; Zhang, Q.; Wu, M.; Huang, Y. Mild Alkaline Pretreatment for Isolation of Native-like Lignin and Lignin-Containing Cellulose Nanofibers (LCNF) from Crop Waste. *ACS Sustainable Chem. Eng.* **2019**, *7*, 14135−14142.

(24) Ämmälä, A.; Laitinen, O.; Sirviö, J. A.; Liimatainen, H. Key Role of Mild Sulfonation of Pine Sawdust in the Production of Lignin Containing Microfibrillated Cellulose by Ultrafine Wet Grinding. *Ind. Crops Prod.* **2019**, *140*, No. 111664.

(25) Dias, M. C.; Belgacem, M. N.; De Resende, J. V.; Martins, M. A.; Damásio, R. A. P.; Tonoli, G. H. D.; Ferreira, S. R. Eco-Friendly Laccase and Cellulase Enzymes Pretreatment for Optimized Production of High Content Lignin-Cellulose Nanofibrils. *Int. J. Biol. Macromol.* **2022**, *209*, 413−425.

(26) Liu, Y.; Chen, W.; Xia, Q.; Guo, B.; Wang, Q.; Liu, S.; Liu, Y.; Li, J.; Yu, H. Efficient Cleavage of Lignin−Carbohydrate Complexes and Ultrafast Extraction of Lignin Oligomers from Wood Biomass by Microwave-assisted Treatment with Deep Eutectic Solvent. *ChemSusChem* **2017**, *10*, 1692−1700.

(27) Wang, H.; Li, J.; Zeng, X.; Tang, X.; Sun, Y.; Lei, T.; Lin, L. Extraction of Cellulose Nanocrystals Using a Recyclable Deep Eutectic Solvent. *Cellulose* **2020**, *27*, 1301−1314.

(28) Cai, C.; Hirth, K.; Gleisner, R.; Lou, H.; Qiu, X.; Zhu, J. Y. Maleic Acid as a Dicarboxylic Acid Hydrotrope for Sustainable Fractionation of Wood at Atmospheric Pressure And≤ 100 C: Mode and Utility of Lignin Esterification. *Green Chem.* **2020**, *22*, 1605−1617.

(29) Zhu, J.; Chen, L.; Cai, C. Acid Hydrotropic Fractionation of Lignocelluloses for Sustainable Biorefinery: Advantages, Opportunities, and Research Needs. *ChemSusChem* **2021**, *14*, 3031−3046.

(30) Cai, C.; Li, J.; Hirth, K.; Huber, G. W.; Lou, H.; Zhu, J. Y. Comparison of Two Acid Hydrotropes for Sustainable Fractionation of Birch Wood. *ChemSusChem* **2020**, *13*, 4649−4659.

(31) Liu, Y.; Chen, B.; Lv, Y.; Ye, X.; Lin, C.; Liu, M. Insight into the Performance of Lignin-Containing Cellulose Nanofibers (LCNFs) via

https://doi.org/10.1021/acs.biomac.3c00515
Biomacromolecules 2023, 24, 3872−3886

Lignin Content Regulation by p-Toluenesulfonic Acid Delignification. *Cellulose* **2022**, *29*, 2273−2287.
(32) Bian, H.; Chen, L.; Dai, H.; Zhu, J. Y. Integrated Production of Lignin Containing Cellulose Nanocrystals (LCNC) and Nanofibrils (LCNF) Using an Easily Recyclable Di-Carboxylic Acid. *Carbohydr. Polym.* **2017**, *167*, 167−176.
(33) Bian, H.; Luo, J.; Wang, R.; Zhou, X.; Ni, S.; Shi, R.; Fang, G.; Dai, H. Recyclable and Reusable Maleic Acid for Efficient Production of Cellulose Nanofibrils with Stable Performance. *ACS Sustainable Chem. Eng.* **2019**, *7*, 20022−20031.
(34) Wise, L. E.; Murphy, M.; Adieco, A. A. D. Chlorite Holocellulose, Its Fractionation and Bearing on Summative Wood Analysis and on Studies on the Hemicelluloses. *Pap. Trade J.* **1946**, *122*, 35−43.
(35) Filipova, I.; Serra, F.; Tarrés, Q.; Mutjé, P.; Delgado-Aguilar, M. Oxidative Treatments for Cellulose Nanofibers Production: A Comparative Study between TEMPO-Mediated and Ammonium Persulfate Oxidation. *Cellulose* **2020**, *27*, 10671−10688.
(36) da Silva Perez, D.; Montanari, S.; Vignon, M. R. TEMPO-Mediated Oxidation of Cellulose III. *Biomacromolecules* **2003**, *4*, 1417−1425.
(37) Tarrés, Q.; Boufi, S.; Mutjé, P.; Delgado-Aguilar, M. Enzymatically Hydrolyzed and TEMPO-Oxidized Cellulose Nanofibers for the Production of Nanopapers: Morphological, Optical, Thermal and Mechanical Properties. *Cellulose* **2017**, *24*, 3943−3954.
(38) Segal, L.; Creely, J. J.; Martin, A. E.; Conrad, C. M. An Empirical Method for Estimating the Degree of Crystallinity of Native Cellulose Using the X-Ray Diffractometer. *Text. Res. J.* **1959**, *29*, 786−794.
(39) Jeong, S.-Y.; Lee, J.-W. Hydrothermal Treatment. In *Pretreatment of Biomass*; Elsevier, 2015; pp 61−74.
(40) Ziegler-Devin, I.; Chrusciel, L.; Brosse, N. Steam Explosion Pretreatment of Lignocellulosic Biomass: A Mini-Review of Theorical and Experimental Approaches. *Front. Chem.* **2021**, *9*, No. 705358.
(41) Fontes, A. M.; Pirich, C. L.; Tanobe, G. R. O. A.; Tarrés, Q.; Delgado-Aguilar, M.; Ramos, L. P. Micro/Nanostructured Lignonanocellulose Obtained from Steam-Exploded Sugarcane Bagasse. *Cellulose* **2021**, *28*, 10163−10182.
(42) Su, C.; Hirth, K.; Liu, Z.; Cao, Y.; Zhu, J. Y. Maleic Acid Hydrotropic Fractionation of Wheat Straw to Facilitate Value-added Multi-product Biorefinery at Atmospheric Pressure. *GCB Bioenergy* **2021**, *13*, 1407−1424.
(43) Maréchal, Y.; Chanzy, H. The Hydrogen Bond Network in Iβ Cellulose as Observed by Infrared Spectrometry. *J. Mol. Struct.* **2000**, *523*, 183−196.
(44) Faix, O. Investigation of Lignin Polymer Models (DHP's) by FTIR Spectroscopy. *Holzforschung* **1986**, *40*, 273−280.
(45) Browning, B. L. *Methods of Wood Chemistry. Volumes I & II*; John Wiley & Sons, Inc, 1967.
(46) Martínez, J. M.; Reguant, J.; Montero, M. Á.; Montané, D.; Salvadó, J.; Farriol, X. Hydrolytic Pretreatment of Softwood and Almond Shells. Degree of Polymerization and Enzymatic Digestibility of the Cellulose Fraction. *Ind. Eng. Chem. Res.* **1997**, *36*, 688−696.
(47) Im, W.; Abhari, A. R.; Youn, H. J.; Lee, H. L. Morphological Characteristics of Carboxymethylated Cellulose Nanofibrils: The Effect of Carboxyl Content. *Cellulose* **2018**, *25*, 5781−5789.
(48) Tyagi, P.; Gutierrez, J. N.; Nathani, V.; Lucia, L. A.; Rojas, O. J.; Hubbe, M. A.; Pal, L. Hydrothermal and Mechanically Generated Hemp Hurd Nanofibers for Sustainable Barrier Coatings/Films. *Ind. Crops Prod.* **2021**, *168*, No. 113582.
(49) Boluk, Y.; Danumah, C. Analysis of Cellulose Nanocrystal Rod Lengths by Dynamic Light Scattering and Electron Microscopy. *J. Nanopart. Res.* **2014**, *16*, No. 2174.
(50) Nechyporchuk, O.; Belgacem, M. N.; Pignon, F. Current Progress in Rheology of Cellulose Nanofibril Suspensions. *Biomacromolecules* **2016**, *17*, 2311−2320.
(51) Hubbe, M. A.; Tayeb, P.; Joyce, M.; Tyagi, P.; Kehoe, M.; Dimic-Misic, K.; Pal, L. Rheology of Nanocellulose-Rich Aqueous Suspensions: A Review. *BioResources* **2017**, *12*, 9556−9661.
(52) Trigui, K.; Magnin, A.; Putaux, J.-L.; Boufi, S. Twin-Screw Extrusion for the Production of Nanocellulose-PVA Gels with a High Solid Content. *Carbohydr. Polym.* **2022**, *286*, No. 119308.
(53) Yuan, T.; Zeng, J.; Wang, B.; Cheng, Z.; Chen, K. Lignin Containing Cellulose Nanofibers (LCNFs): Lignin Content-Morphology-Rheology Relationships. *Carbohydr. Polym.* **2021**, *254*, No. 117441.
(54) French, A. D. Idealized Powder Diffraction Patterns for Cellulose Polymorphs. *Cellulose* **2014**, *21*, 885−896.
(55) Khelil, R.; Jardé, E.; Cabello-Hurtado, F.; Ould-el-Hadj Khelil, A.; Esnault, M.-A. Structure and Composition of the Wax of the Date Palm, Phoenix Dactylifera L., from the Septentrional Sahara. *Sci. Hortic.* **2016**, *201*, 238−246.
(56) Henriksson, M.; Berglund, L. A.; Isaksson, P.; Lindström, T.; Nishino, T. Cellulose Nanopaper Structures of High Toughness. *Biomacromolecules* **2008**, *9*, 1579−1585.
(57) Benítez, A. J.; Walther, A. Cellulose Nanofibril Nanopapers and Bioinspired Nanocomposites: A Review to Understand the Mechanical Property Space. *J. Mater. Chem. A* **2017**, *5*, 16003−16024.
(58) Galland, S.; Berthold, F.; Prakobna, K.; Berglund, L. A. Holocellulose Nanofibers of High Molar Mass and Small Diameter for High-Strength Nanopaper. *Biomacromolecules* **2015**, *16*, 2427−2435.
(59) Sethi, J.; Visanko, M.; Österberg, M.; Sirviö, J. A. A Fast Method to Prepare Mechanically Strong and Water Resistant Lignocellulosic Nanopapers. *Carbohydr. Polym.* **2019**, *203*, 148−156.
(60) Bian, H.; Gao, Y.; Wang, R.; Liu, Z.; Wu, W.; Dai, H. Contribution of Lignin to the Surface Structure and Physical Performance of Cellulose Nanofibrils Film. *Cellulose* **2018**, *25*, 1309−1318.

https://doi.org/10.1021/acs.biomac.3c00515
Biomacromolecules 2023, 24, 3872−3886